THE JOURNAL OF PHYSICAL CHEMISTRY B
A JOURNAL OF THE AMERICAN CHEMICAL SOCIETY

pubs.acs.org/JPCB
Article

Atherosclerotic Oxidized Lipids Affect Formation and Biophysical Properties of Supported Lipid Bilayers and Simulated Membranes

Dane E. Santa,[‖] Turner P. Brown,[‖] Wonpil Im,* and Nathan J. Wittenberg*

Cite This: *J. Phys. Chem. B* 2024, 128, 11694–11704

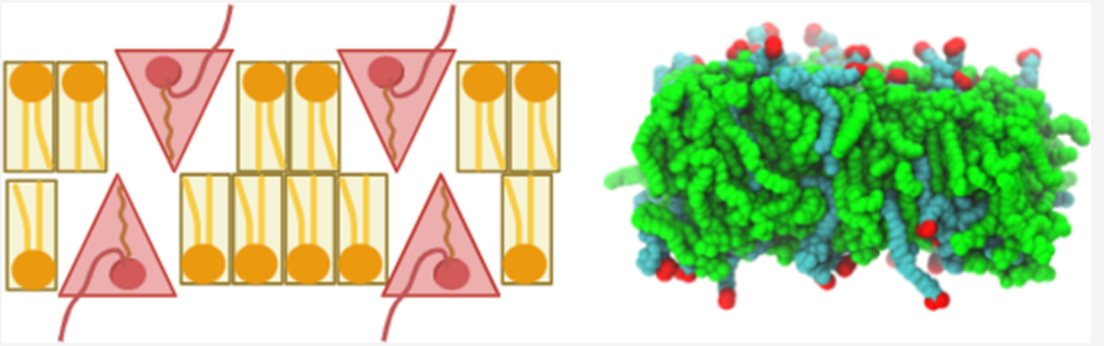

ABSTRACT: Oxidized lipids arising from oxidative stress are associated with many serious health conditions, including cardiovascular diseases. For example, KDdiA-PC and KOdiA-PC are two oxidized phosphatidylcholines (oxPC) directly linked to atherosclerosis, which precipitate heart failure, stroke, aneurysms, and chronic kidney disease. These oxPCs are well-characterized in small particles such as low-density lipoprotein, but how their presence affects the biophysical properties of larger bilayer membranes is unclear. It is also unclear how membrane mediators, such as cholesterol, affect lipid bilayers containing these oxPCs. Here, we characterize supported lipid bilayers (SLBs) containing POPC, KDdiA-PC, or KOdiA-PC, and cholesterol. We used a quartz crystal microbalance with dissipation monitoring (QCM-D), fluorescence microscopy, and all-atom molecular dynamics (MD) to examine the formation process, biophysical properties, and specific lipid conformations in simulated bilayers. Experimentally, we show that liposomes containing either oxPC form SLBs by rupturing on contact with SiO_2 substrates, which differs from the typical adsorption-rupture pathway observed with nonoxidized liposomes. We also show that increasing the oxPC concentration in SLBs results in thinner bilayers that contain defects. Simulations reveal that the oxidized *sn*-2 tails of KDdiA-PC and KOdiA-PC bend out of the hydrophobic membrane core into the hydrophilic headgroup region and beyond. The altered conformations of these oxPC, which are affected by cholesterol content and protonation state of the oxidized functional groups, contribute to trends of decreasing membrane thickness and increasing membrane area with increasing oxPC concentration. This combined approach provides a comprehensive view of the biophysical properties of membranes containing KDdiA-PC and KOdiA-PC at the molecular level, which is crucial to understanding the role of lipid oxidation in cardiovascular disease and related immune responses.

INTRODUCTION

The oxidation of phospholipids that comprise cell membranes is a major consequence of oxidative stress. Small amounts of oxidized phospholipids (oxPL) are critical for normal cell function and serve as immunomodulatory signals for both pro- and anti-inflammatory pathways in response to pathogenic replication and tissue damage.[1] However, an overabundance of oxPLs caused by oxidative stress and chronic inflammation also leads to the damage of critical cellular components and ultimately necrotic and apoptotic cell death.[2−4] Phospholipids that contain polyunsaturated fatty acid (PUFA) tails are highly susceptible to oxidation. Two such examples are 1-palmitoyl-2-linoleoyl-*sn*-glycero-3-phosphocholine (PLPC) and 1-palmitoyl-2-arachidonoyl-*sn*-glycero-3-phosphocholine (PAPC), both of which possess multiple sites of unsaturation in their *sn*-2 chains that can be oxidized, forming numerous oxidized phosphatidylcholine (oxPC) products implicated in disease. For example, oxPC in neuronal membranes and myelin sheaths mediate neurodegeneration in disorders like multiple sclerosis, spinal cord injury, and frontotemporal lobe dementia.[5] In cancer cells, oxPC promotes tumor metastasis by inducing autophagy-mediated endothelial-mesenchymal transition.[6] Importantly, oxPC in cell membranes and oxidized low-density lipoprotein

Received: August 13, 2024
Revised: November 5, 2024
Accepted: November 7, 2024
Published: November 19, 2024

https://doi.org/10.1021/acs.jpcb.4c05451
J. Phys. Chem. B 2024, 128, 11694−11704

(oxLDL) particles are recognized by immune cell scavenger receptors, inducing lipid uptake, promoting foam cell formation, and activating inflammatory pathways associated with atherosclerosis, a key underlying factor for cardiovascular diseases that have been the foremost cause of global mortality for the last century.[7] A core reason for the interrelation is that the biophysical properties of oxPC-containing membranes differ from those of nonoxidized membranes.

Changes in biophysical properties of oxPC-containing membranes result from differing conformations between oxPC and their nonoxidized counterparts. Oxidation reactions in unsaturated lipid acyl tails produce, among other toxic products,[8] truncated acyl chains with polar functional groups.[9] This causes normally hydrophobic *sn*-2 tails to bend into the membrane interfacial region and beyond like tiny "whiskers".[10] The overall effects of these conformational changes are thinner, less densely packed membranes that also exhibit increased permeability, although the effects vary for different oxPCs.[11−15] The effects of several oxPC species on membrane biophysical properties have been studied, but many more oxPC related to disease and subsequent immune responses have yet to be characterized.

Two oxPC involved in cardiovascular disease and inflammatory immune response are 1-palmitoyl-2-(9-oxo-11-carboxy-10*E*-undecenoyl)-*sn*-glycero-3-phosphocholine (KDdiA-PC) and 1-palmitoyl-2-(5-oxo-7-carboxy-6*E*-heptanoyl)-*sn*-glycero-3-phosphocholine (KOdiA-PC) as shown in Figure 1. These

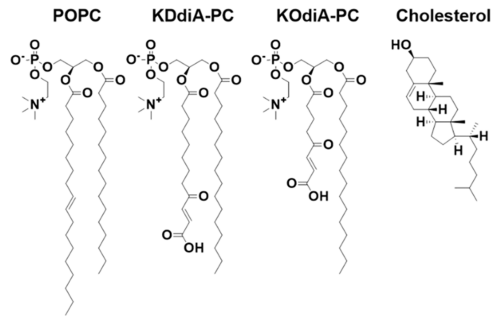

Figure 1. Chemical structures of lipids used in this study: 1-palmitoyl-2-oleoyl-*sn*-glycero-3-phosphocholine (POPC), 1-palmitoyl-2-(9-oxo-11-carboxy-10*E*-undecenoyl)-*sn*-glycero-3-phosphocholine (KDdiA-PC), 1-palmitoyl-2-(5-oxo-7-carboxy-6*E*-heptanoyl)-*sn*-glycero-3-phosphocholine (KOdiA-PC), and cholesterol.

molecules belong to two families of oxPC derived from PAPC and PLPC, respectively.[16] Structurally, the *sn*-3 head groups (phosphatidylcholine) and *sn*-1 tail (palmitic acid) of KDdiA-PC and KOdiA-PC are identical to those of POPC. The *sn*-2 tails of KDdiA-PC and KOdiA-PC are both truncated (KDdiA-PC has 12 carbons, KOdiA-PC has 8 carbons) and include a γ-oxo-α,β-unsaturated carboxylic acid. Combined, the *sn*-2 chains of KDdiA-PC and KOdiA-PC render them as high-affinity ligands for class B scavenger receptors like CD36, which is involved in selective uptake of oxidized forms of LDL (oxLDL) by macrophages as well as macrophage transition to foam cells and atherosclerotic lesion development.[17] Studies including KDdiA-PC and KOdiA-PC focus on oxLDL particles and comparable membrane models,[18,19] but how these oxPCs affect the biophysical properties of bilayer membranes has yet to be investigated in full.

Both experimental and computational methods have been used to study the effects of oxPC on the biophysical properties of the oxidized membranes. Experimentally, surface-sensitive analytical techniques like atomic force microscopy, surface plasmon resonance, optical microscopy, and quartz crystal microbalance with dissipation monitoring (QCM-D) have been used to reveal information about oxidized supported lipid bilayer (SLB) formation via liposome rupture as well as the biophysical characteristics of the SLBs.[20−23] These methods have also been used to show how modulating factors like cholesterol affect membrane biophysical properties.[24,25] Computational studies have also shown the effects of oxPC on bilayer membranes. In general, simulated bilayers that include oxPC are thinner and less densely packed than nonoxidized bilayers.[26−28] These molecular dynamics (MD) simulations also predict the orientation of oxPC molecules in bilayers and provide additional insight into the individual effects of chemically diverse oxPC on lipid bilayers.

This study reports the specific effects of KDdiA-PC and KOdiA-PC on SLB formation and membrane biophysical properties. Experimentally, we use QCM-D and fluorescence microscopy to show that liposomes containing these oxPCs rupture more readily on SiO_2. We also show that oxidized SLBs that contain biologically relevant concentrations of cholesterol are thicker than those that do not contain cholesterol. These results are supported by all-atom MD simulations, which show trends of increasing area per lipid (APL) with increasing oxPC concentration. Overall, this combined experimental and computational approach provides comprehensive insight into what is occurring in oxPC-containing membranes down to the molecular level.

METHODS

Liposome Preparation. KDdiA-PC and KOdiA-PC were purchased from Cayman Chemical. POPC, cholesterol, and nitrobenzoxadiazole (NBD)-labeled PC were purchased from Avanti Polar Lipids. Lipids dissolved in chloroform were combined in desired molar ratios in amber glass vials and desiccated under vacuum for >2 h to evaporate the chloroform. Small unilamellar vesicles were then formed at total lipid concentrations of 1 mg/mL by rehydrating the lipid films in 1 mL of Tris buffer (10 mM Tris base, 250 mM NaCl, 2.2 mM $CaCl_2$, pH 7.0), vortexing to suspend lipids, and sonicating the suspensions in a bath sonicator (Branson) for 10 min at room temperature. Suspended liposomes were then extruded 23 passes through a 50 nm-pore size polycarbonate membrane filter (Cytiva) using an Avanti mini-extruder. KDdiA-PC or KOdiA-PC mole fractions in liposomes were 10, 20, or 30 mol %, respectively. Liposomes with all concentrations of oxPC were prepared with and without 30 mol % cholesterol.

Supported Lipid Bilayer Formation. A QSense Explorer E1 QCM-D instrument (Biolin Scientific) was used to monitor SLB formation. QCM-D sensor chips (Biolin Scientific) were AT-cut SiO_2-coated quartz crystals with a 5 MHz fundamental frequency. Sensors were cleaned by first soaking in 2% SDS for at least 30 min and then rinsing 5 times with ultrapure water. The sensors were then dried under a stream of N_2 gas and placed in a UV-Ozone chamber for 10 min before immediately transferring to the QCM-D flow cell. The instrument allowed for the internal temperature of the flow cell to be held constant at 23.0 °C. Liposomes were diluted to a total lipid concentration of 0.1 mg/mL in Tris buffer (10 mM Tris base, 250 mM NaCl, and 2.2 mM $CaCl_2$, pH 7.0) and flowed through the QCM-D flow cell at a constant rate of 100 μL/min using a peristaltic pump. Upon SLB formation, which was determined by signal stabilization, sensors

https://doi.org/10.1021/acs.jpcb.4c05451
J. Phys. Chem. B 2024, 128, 11694−11704

were washed with Tris buffer (10 mM Tris base, 250 mM NaCl, pH 7.0) at a flow rate of 100 μL/min. In cases where the signals did not stabilize, the flow cell was washed after 10 min of liposome exposure. For each trial, frequency and dissipation were monitored at the first, third, fifth, seventh, ninth, 11th, and 13th overtones. The third overtone was used to model all data reported in this study and to estimate bilayer mass using the modified Sauerbrey equation.[29]

Fluorescence Microscopy. Images of SLB formation were collected in homemade poly(dimethylsiloxane) (PDMS) micro wells bonded to glass coverslips. Coverslips were soaked in 2% (w/v) SDS solution for at least 30 min, rinsed with ultrapure H_2O, and dried with a stream of N_2 gas. Micro wells were formed in PDMS slabs using a 5 mm diameter biopsy punch, which produced wells with a total volume of approximately 100 μL. Both coverslips and PDMS were then treated with air plasma (Harrick Plasma) for 90 s at 280 mTorr and immediately filled with approximately 100 μL of Tris buffer (10 mM Tris base, 250 mM NaCl, and 2.2 mM $CaCl_2$, pH 7.0) after being brought into contact. The wells were then mounted for imaging using total internal reflection fluorescence microscopy (TIRFM; Nikon Eclipse Ti, 100× objective, 1.49 N.A.). Liposomes were diluted to a total lipid concentration of 0.1 mg/mL in Tris (10 mM Tris base, 250 mM NaCl, and 2.2 mM $CaCl_2$, pH 7.0) and added to the wells, while TIRFM images of liposome adhesion and rupture were recorded. Images of SLB formation were acquired at 5 s intervals until stabilization of fluorescence intensity (>10 min). NBD fluorescence was excited using a 488 nm diode laser and a FITC filter set (Chroma). Images were captured with a 2048 × 2048 pixel sCMOS camera (Orca Flash 4.0 v2, Hamamatsu). After SLB formation, wells were washed out with at least 3 mL of Tris (10 mM Tris base, 250 mM NaCl, pH 7.0) and remounted to record fluorescence recovery after photobleaching (FRAP) using epifluorescence. Samples were bleached using a 405 nm laser (50 mW) pulse for 2 s, and fluorescence recovery was recorded at 1 s intervals for 2 min. For FRAP (fluorescence recovery after photobleaching) imaging, NBD fluorescence was excited using an LED light engine (Aura II, Lumencor). Diffusion coefficients of fluorescent lipids were calculated using the Hankel transform and MATLAB script detailed by Jönsson et al.[30] All image analysis was performed using Nikon Elements and ImageJ software.

Computational System Setup. Our all-atom MD simulation systems were built using CHARMM-GUI Membrane Builder.[31−33] Twenty-six compositionally distinct bilayers were built, varying in oxPL concentration, chain length, protonation state, and presence of cholesterol. System details are summarized in Table S1. Two of these twenty-six bilayers are the control systems: 100% POPC bilayer and 70/30% POPC/cholesterol bilayers. Three replicas of each system were made for a total of 78 simulations. For convenience, these systems were named based on the oxPL type, protonation state, concentration, and the presence of 30% cholesterol. For example, the system with 20 mol % deprotonated KOdiA-PC and cholesterol is named dp-KO-20-chol. The CHARMM36m force field was used for all lipids[34] together with the TIP3P water model.[35] A force-switching function[36] was applied to van der Waals interactions over 10−12 Å, and the electrostatic interactions were calculated using the particle-mesh Ewald method.[37] A semi-isotropic Monte Carlo barostat and Langevin Dynamics friction coefficient of 1 ps^{-1} were used to maintain pressure (1 bar) and temperature (310 K), respectively. Reutilizing the input scripts generated by Membrane Builder,[38] including the six-step Membrane Builder equilibration process,[33] we used OpenMM software[39] to perform all simulations with a 4 fs time-step utilizing the hydrogen mass repartitioning technique[40] and the SHAKE algorithm.[41]

Simulation Analysis Methods. Membrane thickness was defined as the average distance along the *Z*-axis between phosphorus atoms in the upper and lower leaflets and was calculated every 0.1 ns for the duration of the production. Density profiles were calculated for various atom types and molecules. POPC headgroup density was defined as the average position of the phosphorus atoms in the head groups. Water density was defined as the average position of the oxygen atoms. Cholesterol density was defined as the average position of the O3 atom. Area per lipid was calculated by first choosing representative atoms from each lipid. For oxidized lipids and POPC, the representative atoms were C21 (first carbon on the *sn*-2 acyl chain), C2 (central carbon in the glycerol backbone), and C31 (first carbon on the *sn*-1 acyl chain). For cholesterol, the representative atom was atoms O3. Each lipid's representative atoms were treated as Voronoi centers. Next, Voronoi tessellation was performed on each frame of the simulation from 0.5 to 1 μs to obtain Voronoi cells. Finally, the average Voronoi cell area (i.e., area per lipid) for each lipid type was calculated. Order parameters were calculated for the carbon atoms of the sn-1 chains of each lipid type according to the following equation: $S_{CD} = |1/2\langle 3\cos^2\theta - 1\rangle|$, where θ is the angle between the direction of the C−H bond and the bilayer normal. Order parameters were averaged over the last 100 ns of each simulation. Lateral diffusion coefficients of POPC were estimated using the method described by Klauda et al.[42] First, the mean-squared displacement (MSD) was obtained by unwrapping the simulation trajectories from the last 100 ns of production. This was done to prevent large displacement values for lipids that move across the periodic boundary. Then, the lateral MSD was calculated for phosphorus atoms of POPC. Finally, for every 10 ns, the lateral diffusion coefficients were estimated by the Einstein Relation: $D = 1/4 \times \mathrm{MSD}/t$.

RESULTS AND DISCUSSION

oxPCs Alter SLB Formation and Biophysical Properties. We used QCM-D to monitor SLB formation by the adsorption and rupture of POPC liposomes containing increasing concentrations of KDdiA-PC or KOdiA-PC on SiO_2. This technique utilizes an oscillating quartz sensor to measure shifts in resonant frequency (ΔF), which is proportional to mass adsorbed to the sensor, and dissipation (ΔD), which is a measure of the viscoelasticity of the adsorbed mass. Figure 2 shows ΔF and ΔD traces over time for liposomes containing increasing concentrations (10−30 mol %) of KDdiA-PC (Figure 2a,c) and KOdiA-PC (Figure 2b,d). Liposomes composed solely of POPC (Figure 2a−d, black traces) exhibited a classical two-step SLB formation process. Initially, the ΔF decreased and the ΔD increased as intact liposomes adsorbed to the sensor until a critical point of surface coverage was achieved. At the critical point, ΔF and ΔD shifted back toward baseline as the liposomes ruptured and released their aqueous contents. The signals then stabilized at values ($\Delta F = -26.5 \pm 0.9$ Hz, $\Delta D = 0.4 \pm 0.3 \times 10^{-6}$) that agree with literature values ($\Delta F = -28$ Hz, $\Delta D = 0.6 \times 10^{-6}$) for a SLB composed of POPC.[43]

Increasing the mole fraction of KDdiA-PC in the liposomes (Figure 2a,c) transformed the SLB formation to a one-step process, where liposomes rupture immediately upon adsorption. The evidence for this is a diminished critical point for

https://doi.org/10.1021/acs.jpcb.4c05451
J. Phys. Chem. B 2024, 128, 11694−11704

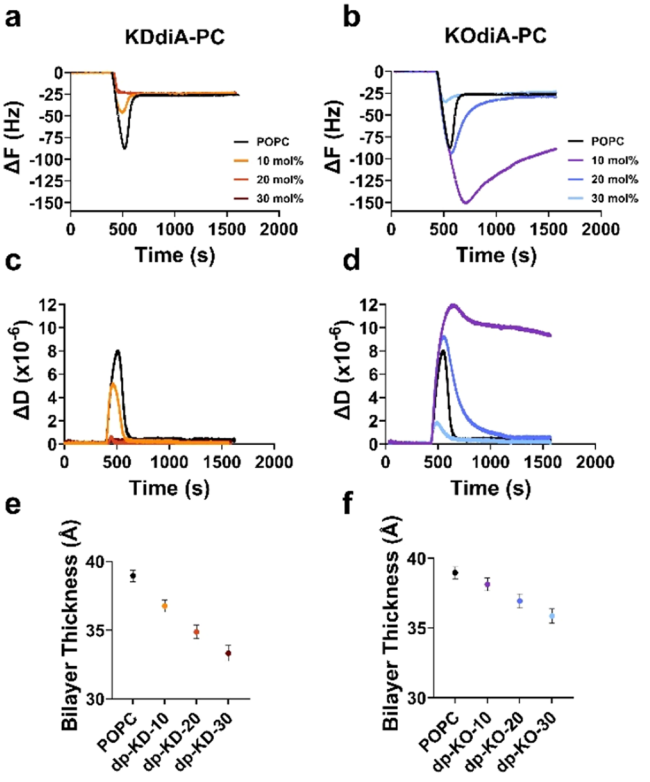

Figure 2. Increasing the oxPC concentration in liposomes affects bilayer formation and alters biophysical properties of formed membrane models. Shifts in resonant frequency (ΔF) and dissipation (ΔD) are shown for the rupture of POPC liposomes with and without KDdiA-PC (a, c) and KOdiA-PC (b, d) over time. Thickness measurements from the simulations of POPC bilayers containing increasing concentrations of KDdiA-PC (e) and KOdiA-PC (f) with deprotonated (dp) carboxylic acids on the *sn*-2 tails. KD represents KDdiA-PC and KO represents KOdiA-PC. The numbers represent the mole fractions of the oxPCs in the simulated compositions. Error bars represent the standard errors of triplicate measurements.

suspensions containing 10 mol % KDdiA-PC vs POPC alone and a direct shift from baseline to stable SLB values at 20 and 30% oxPC concentrations. Similar transitions from two-step to one-step bilayer formation have been observed using QCM-D to monitor the rupture of POPC liposomes containing increasing concentrations of other oxidized PCs, such as PAze-PC and poxno-PC on SiO_2.[14,44] Liposomes containing 30 mol % KOdiA-PC (Figure 2b,d) also showed diminished critical point ΔF and ΔD values; although at lower concentrations, the critical ΔF and ΔD values were larger than for POPC alone and they did not stabilize for liposomes containing 10 mol % KOdiA-PC. We attribute the increasing trend of excessive signals with lower KOdiA-PC concentration to intact liposomes adsorbing on the SLB formed on the QCM-D sensors. We surmise that the liposomes containing 20 mol % KOdiA-PC (more so at 10 mol % KOdiA-PC) retain some character of nonoxidized POPC. This makes them stable enough not to rupture on contact but "sticky" due to protruding oxidized *sn*-2 chains, which are free to interact with the SLB. Regardless, the observed one-step SLB formation indicates that the KDdiA-PC liposomes rupture on contact with the sensor instead of remaining intact until a critical surface coverage is reached.[44] Ruptured liposomes form "patches" of incomplete SLB. The exposed hydrophobic edges of these patches catalyze further liposomal rupture to form a complete SLB, which is more energetically favorable.[45]

The rupture of liposomes containing zwitterionic lipids such as POPC is predominantly driven by adhesion and deformation forces between liposomes and the SiO_2 substrate overtaking the cohesive intermolecular forces that maintain liposomal structures. It is likely that the lipid conformational differences in liposomes with KDdiA-PC disrupt lipid packing order, which weakens the cohesive forces in liposomes and results in spontaneous rupture upon surface contact. Shifts in ΔF can be used to obtain measurements for areal mass adsorbed to the sensor surface, which is a product of the lipid density and thickness of an SLB; however, oxPCs can induce membrane defects, making direct thickness measurements with QCM-D challenging. For this reason and the excess signal observed for SLBs containing KOdiA-PC, we used MD simulations to calculate the thickness of lipid bilayers containing deprotonated oxPCs. The membrane thickness was measured as the mean distance between the phosphate groups across the membrane bilayer. For SLBs containing either KDdiA-PC (Figure 2e) or KOdiA-PC (Figure 2f), there is a trend of decreasing bilayer thickness with increasing oxPC concentration, which agrees with previous studies of oxPC in bilayer simulations.[27,28,46] Furthermore, KDdiA-PC has a more pronounced thinning effect than KOdiA-PC. We attribute this enhanced membrane thinning to differences in oxidized chain length between the oxPCs, which has been previously shown to greatly affect membrane thickness. The 4 additional carbons in the *sn*-2 chain of KDdiA-PC presumably disrupt lipid packing more than KOdiA-PC, resulting in thinner membranes with increasing oxPC concentration.

Cholesterol Modulates the Effects of oxPC on SLB Formation. We also used QCM-D to explore the modulatory effect of cholesterol in SLBs containing KDdiA-PC or KOdiA-PC. Cholesterol constitutes a large fraction of total lipids in mammalian cell membranes and plays a key role in maintaining membrane biophysical characteristics, including fluidity and permeability. Figure 3 shows ΔF and ΔD traces over time (a−d) for POPC liposomes containing 30 mol % cholesterol and 10−30 mol % KDdiA-PC (a,c) or KOdiA-PC (b,d). Again, increasing KDdiA-PC (Figure 3a,c) in liposomes shifted bilayer formation from a two-step to a one-step process, evidenced by the direct shift in ΔF and ΔD from baseline to stable SLB values. One-step bilayer formation was also observed for liposomes containing cholesterol and 30 mol % KOdiA-PC. At lower concentrations (10, 20 mol %) of KOdiA-PC, the magnitude of ΔF and ΔD increased indefinitely when flowing liposomes over the sensor, and the signals remained stable upon switching to the washing buffer. MD simulations again show a trend of decreasing bilayer thickness with increasing KDdiA-PC (Figure 3e) and KOdiA-PC (Figure 3f) concentration. Additionally, bilayers containing cholesterol are 14.7−15.9% thicker than the corresponding cholesterol-free bilayers at each oxPC concentration (Figure 2e,f).

The increased membrane thickness observed in systems containing cholesterol can be explained by cholesterol's ability to modulate membrane biophysical characteristics through hydrogen bonding interactions between the 3β−OH of cholesterol and oxygens in surrounding lipids.[47,48] The oxidized moieties of KDdiA-PC and KOdiA-PC cause the *sn*-2 chains to bend into the hydrophilic headgroup region of the membrane and further into the aqueous surroundings. These conformational changes typically result in reduced lipid density (in the hydrophobic membrane core) and membrane thinning as the oxidized lipids have a greater lateral footprint and cannot pack

https://doi.org/10.1021/acs.jpcb.4c05451
J. Phys. Chem. B 2024, 128, 11694−11704

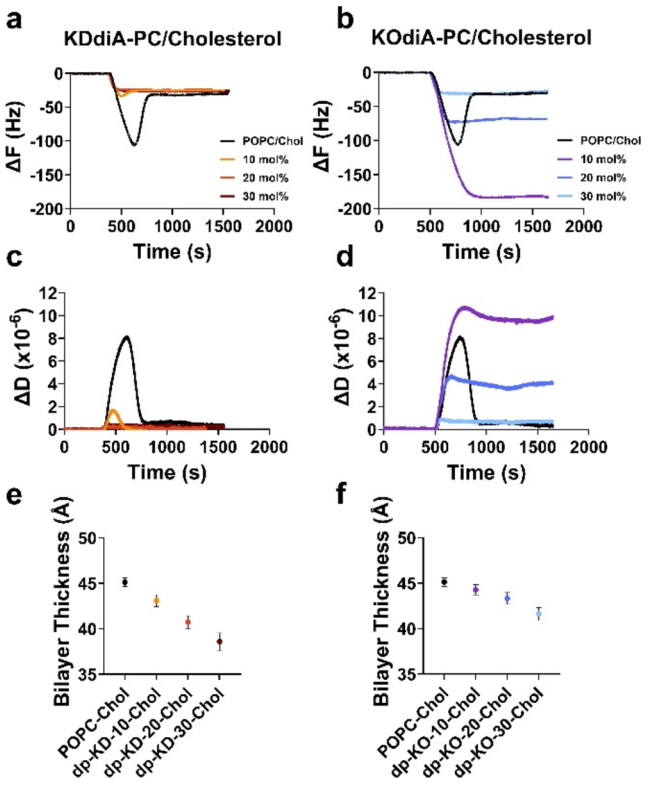

Figure 3. Cholesterol modulates the bilayer formation and biophysical properties of membrane models containing increasing oxPC concentrations. Shifts in resonant frequency (ΔF) and dissipation (ΔD) are shown for POPC liposomes containing 30 mol % cholesterol as well as KDdiA-PC (a, c) and KOdiA-PC (b, d) over time. Thickness measurements from the simulations of POPC bilayers containing 30 mol % cholesterol and increasing concentrations of KDdiA-PC (e) and KOdiA-PC (f) with deprotonated (dp) carboxylic acids on their *sn*-2 tails. KD represents KDdiA-PC and KO represents KOdiA-PC. The numbers represent the mole fractions of the oxPCs in the simulated compositions. Error bars represent the standard errors of triplicate measurements.

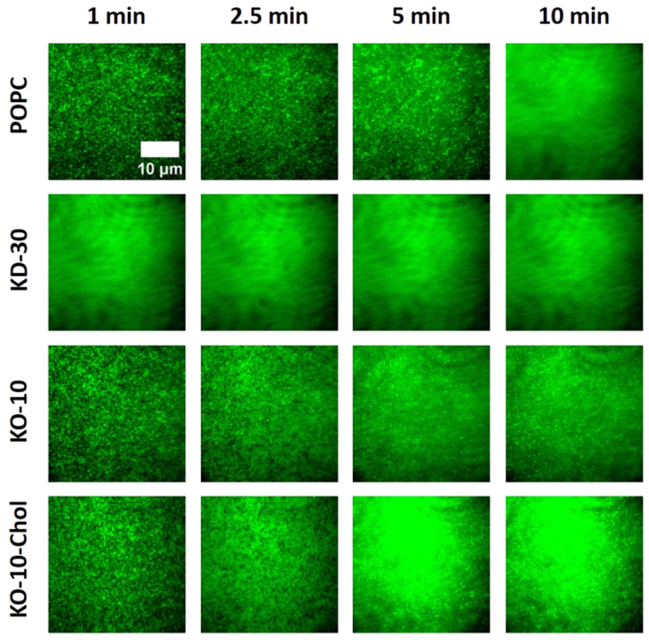

Figure 4. Increasing the oxPC concentration alters SLB formation. Fluorescent micrographs of liposome adsorption and rupture on glass coverslips for samples containing (top to bottom) POPC/NBD-PC (98:2), POPC/KDdiA-PC/NBD-PC (68:30:2), POPC/KOdiA-PC/NBD-PC (88:10:2), and POPC/KOdiA-PC/Cholesterol/NBD-PC (58:10:30:2). Images are 512 × 512-pixel sections taken from micrographs contained in Supporting Movies S1−S4. See the Supporting Information for imaging details.

together as tightly as nonoxidized lipids alone. In the presence of cholesterol, the polar oxidized chains are available to hydrogen bond with cholesterol 3β−OH groups. This has been seen previously in simulated models containing POPC, PGPC (*sn*-2 tail contains 5 carbons and a terminal carboxylic acid), and cholesterol. In these systems, the oxidized tail of PGPC pokes out into the headgroup region. The hydroxyl groups of cholesterol preferentially hydrogen bind with the terminal carboxylic acids of PGPC and fill the corresponding vacancy in the hydrophobic core.[49] In our systems, these interactions tether the oxidized lipids in place and allow them to pack more tightly in the membrane, resulting in increased membrane thickness.

Fluorescence Imaging of SLB Formation. We used TIRF microscopy to further examine the formation of SLBs from liposomes containing KOdiA-PC or KDdiA-PC. Figure 4 shows examples of liposome rupture over the course of 10 min for samples with increasing oxPC concentrations and a fluorescent reporter (NBD-PC). Full time-lapse movies of fluorescent micrographs are supplied in Movies S1−S4. Micrographs of nonoxidized liposomes (Figure 4 and Movie S1) show individual punctules of light accumulating on the coverslip before the point of critical coverage and after which a large majority of the punctules are replaced by a field of uniform fluorescence intensity. This confirms the two-step SLB formation process previously shown by other groups.[43,50] In contrast, micrographs of liposomes containing KDdiA-PC (Figure 4 and Movie S2) rapidly form a nonuniform field of fluorescent patches with distinct defects that fuse over time. One-step SLB formation via oxidized liposome rupture has not been observed fluorescently although the formation of SLBs with numerous defects agrees with the tendency of oxPC to induce and stabilize membrane defects.[14,15,51] The normalized fluorescence intensity of Movies S1 and S2 over time, shown in Figure S1, further illustrates the difference between one- and two-step SLB formations. For POPC liposomes (black trace), adsorption of the liposomes begins with an increase in fluorescence intensity followed by a distinct decrease at approximately 320 s. This decrease corresponds to the rupture cascade visualized in Movie S1 and is similar to the results reported by Fygenson and co-workers.[45] The fluorescence intensity decline is absent for liposomes containing 30 mol % KDdiA-PC (light blue trace) and supports a mechanism by which liposomes rupture upon contact with the substrate.

Interestingly, liposomes that contain KOdiA-PC (Figure 4 and Movie S3) rupture to form fluorescent fields with distinct punctules in the foreground, and the effect is enhanced for liposomes including additional cholesterol (Figure 4 and Movie S4). This confirms that the ΔF and ΔD traces observed in Figures 2 and 3 are the result of intact liposomes binding to a formed SLB containing KOdiA-PC. Although more studies are needed to discern why liposomes containing KOdiA-PC and not KDdiA-PC bind to formed SLBs, this is possibly due to the structural differences in their oxidized *sn*-2 chains contributing to competing hydrophobic and hydrophilic forces in the membrane. How an oxPC behaves in membrane model systems is characteristic of individual species and is a function of their

https://doi.org/10.1021/acs.jpcb.4c05451
J. Phys. Chem. B 2024, 128, 11694−11704

chain length and oxidized moiety.[52] The two oxPCs in this study are structurally identical, aside from the length of their *sn*-2 acyl chains. For this reason, we propose that the 4 additional carbons of KDdiA-PC strengthen hydrophobic interactions with the acyl core and therefore anchor the *sn*-2 chain in the membrane. The *sn*-2 chain of KOdiA-PC, which is 4 carbons shorter, is less anchored and therefore more able to extend into the hydrophilic headgroup region and further into the aqueous medium.

Effects of oxPC Concentration on Lipid Lateral Diffusion in Bilayers. To probe the effects of the oxPC concentration on the lateral diffusivity of fluorescent reporters in SLBs, we conducted fluorescence recovery after photobleaching (FRAP). Figure 5 shows average diffusion coefficients for SLBs

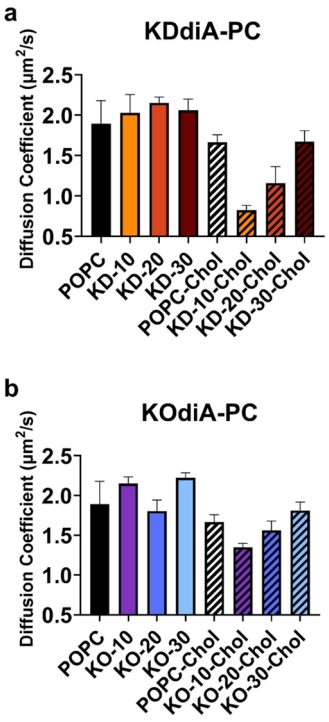

Figure 5. Increasing the oxPC concentration affects lipid lateral diffusion in SLBs. Experimentally measured diffusion coefficients for SLBs containing KDdiA-PC (a) and KOdiA-PC (b) on glass coverslips. Values for POPC/oxPC bilayers are shown as solid colors, and values for those containing 30 mol % cholesterol are shown with black stripes. Error bars represent the standard deviation of triplicate measurements.

containing NBD-PC with increasing concentrations of KDdiA-PC (a) or KOdiA-PC (b) both without and with 30 mol % cholesterol. There are no significant trends in diffusivity for SLBs containing KDdiA-PC or KOdiA-PC alone (circles), but the addition of cholesterol (diamonds) results in a lower diffusion coefficient for every SLB composition. In cholesterol-containing systems, there is also a trend of increasing diffusion coefficient with increasing oxPC concentration. Studies that report the effects of oxPC on lateral diffusion in membrane models vary; the effects of oxPC on lateral diffusion in membranes are largely unique to different oxPC species.[53] To this point, Beranova et al. show increased rates of diffusion in large unilamellar vesicles incorporating POPC and 10 mol % oxPC with truncated *sn*-2 chains (POV−PC and PGPC),[26] but Paez−Perez and colleagues report decreasing diffusion coefficients in MD simulations with increasing amounts of full-chain peroxidated POPC.[54] Similarly, enzymatically oxidized SLBs display lower lipid diffusion coefficients.[55] Also, the correlation between decreasing diffusion coefficients and increasing cholesterol concentration is well established in models containing non-oxidized PC only[56] as well as oxPC.[57]

We attribute the experimentally observed trends of increasing diffusion coefficients with increasing oxPC concentrations in cholesterol-containing SLBs to competing lipid−lipid interactions affecting the area per lipid (APL) in the SLBs. Larger APL values are correlated with faster lipid lateral diffusion because individual lipids have more space to move, albeit lateral diffusion in membranes is a complex process affected by many factors (molecular structure, overall lipid composition, model system used, solvent viscosity and ionic strength, temperature, etc.).[58] Figure S2 shows the average APL from the simulations containing increasing KDdiA-PC (a) and KOdiA-PC (b) concentrations with (diamonds) and without cholesterol (circles). Our simulations reveal two phenomena. First, incorporating oxPC in simulations results in a larger average APL, which has been observed elsewhere.[28,46] Second, adding cholesterol to each lipid composition in simulations results in a smaller average APL, which has also been established in literature.[59] Taken together, the increases in average APL caused by oxPC conformational changes outweigh the decreases in average APL caused by hydrogen bonding between cholesterol and lipid head groups (and polar tails in the case of oxPC) as the oxPC concentration increases. Furthermore, the previously mentioned structural differences between the oxPC explain why this effect is more pronounced with KDdiA-PC versus KOdiA-PC. It is important to note that diffusion coefficients calculated from simulations shown in Figures S3 and S4 are not in strict alignment with experimental values but show similar trends. We attribute this difference to a lack of lipid−substrate interactions in our computational models in comparison to the experimental SLBs and the tendency for simulations to overestimate diffusion values;[60,61] however, further experimentation is required to discern why the disagreement is occurring.

Molecular Dynamics Simulations of Bilayers with oxPCs. QCM-D and FRAP are important experiments for elucidating the bilayer formation mechanisms of oxPC-containing bilayers. However, some bilayer properties, such as the membrane thickness or the positions of specific atoms, are challenging to measure using traditional experimental techniques. MD simulations were performed to determine these properties and investigate the bilayers on smaller time scales. Simulated bilayers mimicking the experimental SLB compositions were made with CHARMM-GUI Membrane Builder[52] (see Methods section). In addition, systems with oxPCs that possess either protonated or deprotonated terminal carboxylic acids were simulated. In total, 78 systems were simulated (Table S1). Our naming scheme for simulated systems indicates the protonation state of the carboxylic acid on the *sn*-2 chain of the oxPC (protonated = p; deprotonated = dp), the identity of the oxPC (KDdiA-PC = KD; KOdiA-PC = KO), the mole fraction of the oxPC, and whether 30 mol % cholesterol is present in the system. For example, the system with 20 mol % deprotonated KDdiA-PC and cholesterol is named dp-KD-20-chol. Figure 6 shows snapshots of the four systems at 2 μs. The simulated bilayers reached dynamic equilibrium soon after equilibration and remained stable for the duration of production (Figure S5).

Effects of Increased oxPC on Simulated Bilayers. System size, membrane thickness, POPC APL, lipid-order parameter, and lateral diffusivity were calculated for all simulated

https://doi.org/10.1021/acs.jpcb.4c05451
J. Phys. Chem. B 2024, 128, 11694−11704

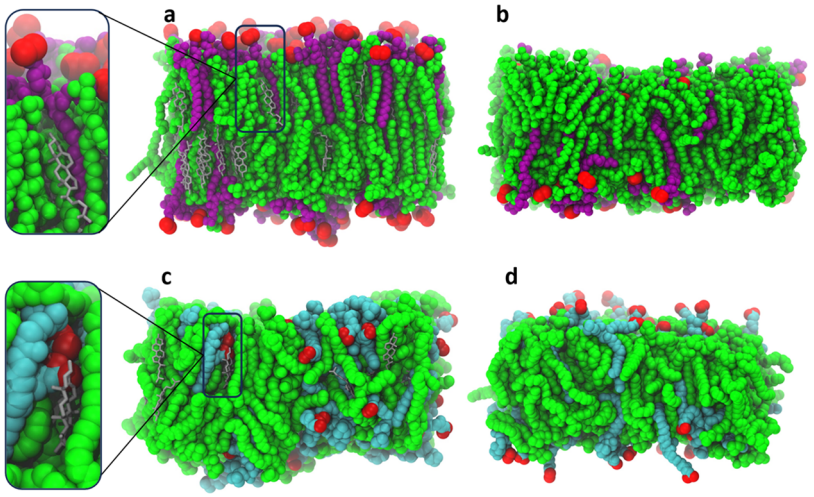

Figure 6. Snapshots from the end of simulations with water and ions omitted for clarity. System names: (a) dp-KO-20-chol, (b) p-KO-20, (c) p-KD-20-chol, and (d) dp-KD-20. Red spheres are carboxyl groups on oxPCs. Green spheres are POPC. Magenta spheres are KOdiA-PC. Cyan spheres are KDdiA-PC. Gray lines are cholesterol.

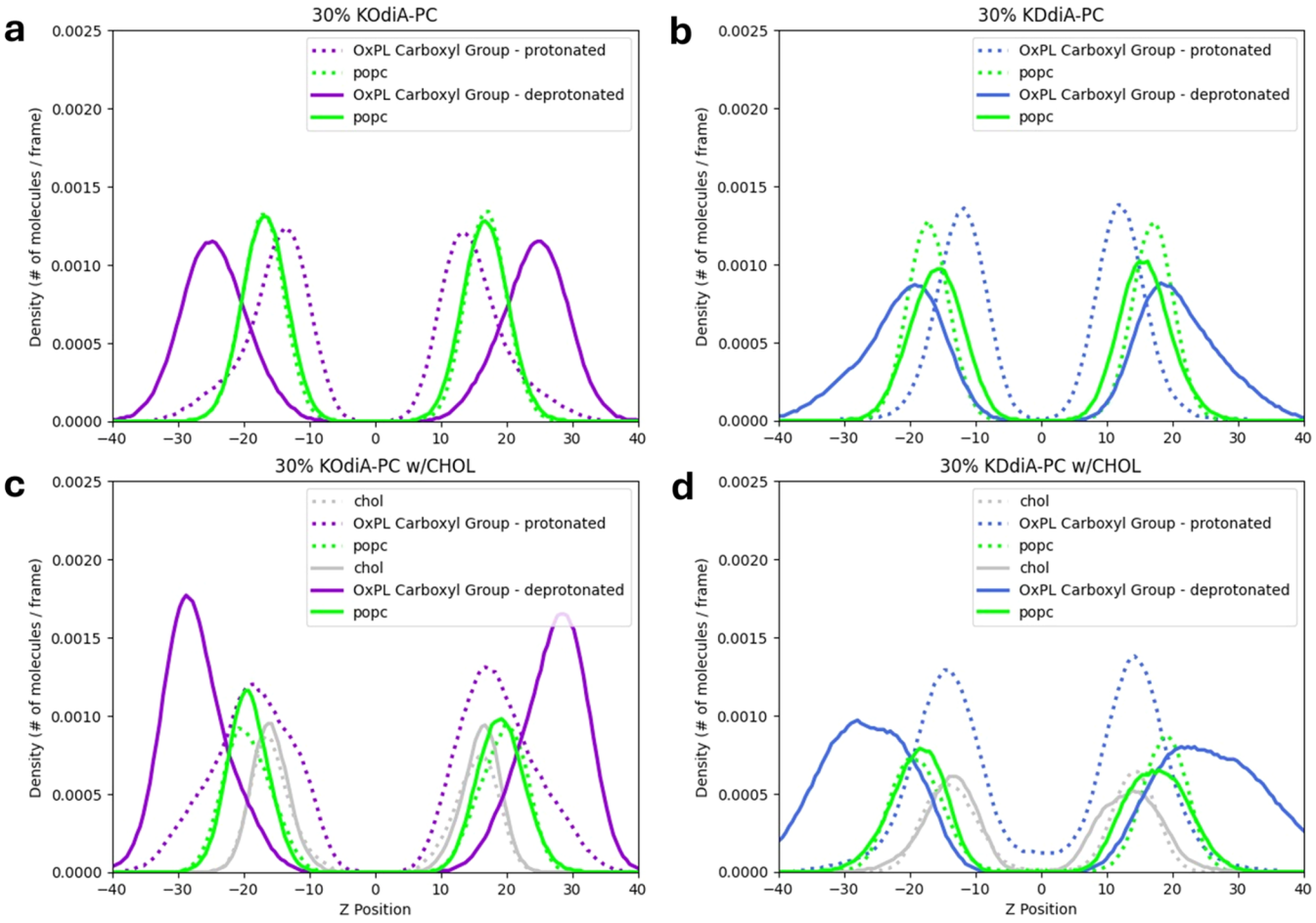

Figure 7. Density profiles along the *Z*-axis (i.e., the membrane normal with the membrane center at $Z = 0$) with 30% oxPC: (a) dp-KO-30 and p-KO-30, (b) dp-KD-30 and p-KD-30, (c) dp-KO-30-chol and p-KO-30-chol, and (d) dp-KD-30-chol and p-KD-30-chol.

bilayers to compare modulations of biophysical properties by oxPC. As seen in the experimentally examined SLBs, these properties depend on the concentration and specific chemistry of oxPC, as well as the presence of cholesterol. APL calculations were performed to quantify how much bilayer expansion occurs at increasing oxPC concentration (Figure S2). In most cases, oxPCs have larger membrane areas (i.e., $X = Y$ membrane area with the membrane normal along the *Z*-axis) than POPC molecules (Figure S5). The one exception is deprotonated KOdiA-PC, which has about the same *XY* area as POPC. Generally, increasing oxPC concentration increases the system size along the *X*-axis, decreases thickness, and decreases the *sn*-1

https://doi.org/10.1021/acs.jpcb.4c05451
J. Phys. Chem. B 2024, 128, 11694−11704

chain order parameter (Figures S5−S8). However, a more complex effect emerges when considering the oxPC chain length. For instance, increasing 12-carbon oxPC (KDdiA-PC) concentration in cholesterol-containing bilayers has a smaller effect on the bilayer thickness compared to cholesterol-free systems (Figure 3e,f). Additionally, lipid-order parameters decrease less dramatically upon addition of KOdiA-PC when compared to KDdiA-PC addition (Figures S6−S7). The presence of oxPC did not have a significant effect on the lateral diffusion of POPC (Figure S4). Overall, the oxidized membranes are wider and thinner than pure POPC membranes, suggesting that phospholipid oxidation induces membrane instability.

To characterize the influence of the protonation state on lipid chain positioning, we compared the *Z*-position of various lipid groups between protonated oxPC and deprotonated oxPC systems. As shown in Figure 7a,b, protonated carboxyl groups on KOdiA-PC and KDdiA-PC settle just inside of POPC head groups, whereas deprotonated carboxyl groups settle outside of the POPC head groups (see also Figure 6). Despite being four methylene units shorter, deprotonated KOdiA-PC's truncated chain reaches just as far into the aqueous space as KDdiA-PC's longer truncated chain. Reversal of the oxPCs *sn*-2 chains pushes adjacent lipids apart and creates more space in the hydrophobic region of the membrane, causing a lower order of the lipids. This is confirmed by a consistent decrease in order parameter with respect to oxPC concentration (Figures S6 and S7). As these truncated chains extend into the aqueous space, hydrophobic forces act on the nonpolar acyl chains, pulling them back toward the water-membrane interface. This phenomenon has been observed in previous studies and is known as the "lipid whisker" model of oxidized membranes.[10,59] This, coupled with the APL analysis, suggests that oxPCs adopt a conical shape within the bilayer. As the concentration of oxPC increases, more lipid tails are positioned near the water-bilayer interface, causing lateral expansion and thinning of the bilayer. Extension of deprotonated tails into the aqueous space suggests that bilayers with oxidized lipids may easily attract scavenger proteins, which can bind to the "lipid whiskers".

Effects of Cholesterol on Simulated Bilayers. To investigate the effects of cholesterol on the membrane properties of bilayers containing various oxPCs, bilayers with 30 mol % cholesterol were simulated for 2 μs. As shown in Figures S3 and S4, addition of cholesterol condenses the pure POPC bilayer, inducing tighter lipid packing and lower membrane area. The current hypothesis is that cholesterol is able to settle into the space left by oxPC chain reversal, reducing lateral pressure and inducing tighter lipid packing.[62] As shown in Figure 6, our simulations confirm this behavior. Cholesterol molecules, colored gray, sit in pockets created by the reversal of oxidized lipid chains. To corroborate with the snapshots, as shown in Figure 7, the *Z*-positions of cholesterol are just inside those of POPC. Average membrane thickness and system size for cholesterol-containing bilayers are listed in Table S2. The presence of cholesterol significantly decreases membrane thickness, while increasing lipid-order parameter compared to cholesterol-free bilayers (Figures S6 and S7). Additionally, cholesterol induces lower APL and lower lipid diffusivity in all bilayers (Figures S2−S6). These results indicate a complex condensing effect by cholesterol, which may help stabilize the bilayer in response to lipid oxidation. Taken together, the bilayer simulations of various oxPC species, concentrations, and cholesterol-containing membranes yield a finely detailed profile of the modulation of bilayers by oxidized lipids.

CONCLUSIONS

In summary, the results from our experiments and simulations indicate that increasing the concentration of atherosclerotic oxidized lipids affects the bilayer formation and biophysical properties of membrane model systems. Increasing KDdiA-PC or KOdiA-PC concentration in liposomes shifts the bilayer formation process from a two-step accumulation rupture to a one-step rupture-on-contact pathway, and formed SLBs containing either oxPC are thinner and less densely packed than those containing POPC. Simulations of POPC bilayers containing KDdiA-PC or KOdiA-PC show trends of decreasing bilayer thickness, increasing membrane area, and increasing APL with increasing oxPC concentration. We also report discrete differences in *sn*-2 tail conformation caused by the protonation state of the contained oxidized moiety. Additionally, incorporating biologically relevant concentrations of cholesterol in both SLBs and simulated bilayers mitigates the effects of an increased oxPC concentration. Overall, combining experimental and computational methods provides a comprehensive view down to the molecular level of what is occurring in bilayer membranes containing oxidized lipids associated with cardiovascular disease.

It is important to note that SLBs and simulations differ from biological membranes in several ways. Most notably, our models are highly simplified in comparison to actual cell membranes that contain vast numbers of different molecules, which may alter the interactions and perturb measurements reported in this study. Additionally, the silica on which our SLBs were formed is much harder than both the extracellular matrix and the cytosol that surround plasma membranes, and our models are not tethered to cytoskeletal filaments. These differences in support structure result in different bilayer-substrate interactions, which can affect both the molecular distribution and overall lateral diffusion. When the reliability of MD simulations is considered, multiple limitations must be noted. First, the accuracy of a simulation relies heavily on the quality of the force field. Despite significant efforts in fine-tuning the parameters of various molecular force fields over decades, no classical force field parameters can perfectly reflect in vivo observations. However, with proper system preparation, force fields (energy functions), and statistical mechanics, the simulation can be used to calculate various experimental observables for direct comparison, validating the simulation. Additionally, the computational resources needed to perform all-atom simulations strongly limit the size and time scale of the study. For instance, our simulated bilayers were about 90 to 100 Å wide, so bilayer properties that require a large lateral area, such as curvature, are difficult to estimate. Finally, because the simulations are ensembles of bilayer conformations at discrete time points, any bilayer properties calculated will be estimations. To alleviate this, we report averages over many time points for all of the estimated properties.

Despite these limitations, our findings have broader implications for biological systems and lay the foundation for future studies of the effects of oxPC in lipid bilayer membranes. Here, we show that increasing concentrations of these oxPC affect bilayer thickness and overall lipid density, which may affect other properties, including membrane permeability and leaflet asymmetry. We also show that cholesterol mitigates the influence of oxPC on the bilayer integrity. If more cholesterol allows for stable membranes with higher oxPC content in vivo,

https://doi.org/10.1021/acs.jpcb.4c05451
J. Phys. Chem. B 2024, 128, 11694−11704

any downstream effects controlled by oxPC concentration (e.g., inflammation and foam cell formation) may be modulated by both the cholesterol and oxPC content. Our studies pave the way for future investigations on how membrane cholesterol could potentially influence scavenger-receptor-mediated cellular responses to oxPCs such as KOdiA-PC and KDdiA-PC.

■ ASSOCIATED CONTENT

Supporting Information

The Supporting Information is available free of charge at https://pubs.acs.org/doi/10.1021/acs.jpcb.4c05451.

Normalized fluorescence of SLB formation (Figure S1); simulation APL (Figure S2); simulated POPC diffusion coefficients (Figure S3); simulated oxPC diffusion coefficients (Figure S4); simulation system sizes (Figure S5); lipid order parameters (Figures S6 and S7); simulated membrane thickness (Figure S8); and MD simulation details and statistics (Tables S1 and S2) (PDF)

Micrographs of POPC liposomes forming a SLB (Movie S1) (AVI)

Micrographs of liposomes that contain KDdiA-PC forming a SLB (Movie S2) (AVI)

Micrographs of liposomes that contain KOdiA-PC forming a SLB (Movie S3) (AVI)

Micrographs of liposomes that contain KOdiA-PC and 30 mol% cholesterol forming a SLB (Movie S4) (AVI)

■ AUTHOR INFORMATION

Corresponding Authors

Wonpil Im − *Department of Biological Sciences, Lehigh University, Bethlehem, Pennsylvania 18015, United States;* orcid.org/0000-0001-5642-6041; Email: wonpil@lehigh.edu

Nathan J. Wittenberg − *Department of Chemistry, Lehigh University, Bethlehem, Pennsylvania 18015, United States;* orcid.org/0000-0001-9196-1867; Email: njw@lehigh.edu

Authors

Dane E. Santa − *Department of Chemistry, Lehigh University, Bethlehem, Pennsylvania 18015, United States;* orcid.org/0000-0003-1337-0396

Turner P. Brown − *Department of Bioengineering, Lehigh University, Bethlehem, Pennsylvania 18015, United States;* orcid.org/0009-0008-5100-629X

Complete contact information is available at: https://pubs.acs.org/10.1021/acs.jpcb.4c05451

Author Contributions

‖D.E.S. and T.P.B. contributed equally to this work. D.E.S. and N.J.W. designed experiments, D.E.S. carried out the experiments, D.E.S. and N.J.W. analyzed experimental data, T.P.B. and W.I. designed simulations, T.P.B. carried out the simulations, T.P.B. and W.I. analyzed simulation data, D.E.S, T.P.B., W.I., and N.J.W. wrote the manuscript.

Notes

The authors declare no competing financial interest.

■ ACKNOWLEDGMENTS

D.E.S., T.P.B., W.I., and N.J.W. acknowledge funding from a Faculty Innovation Grant from Lehigh University (Award number FIGAWD1542). D.E.S. is supported by a National Science Foundation Graduate Research Fellowship. W.I. also acknowledges support from the National Science Foundation (Award number 2111728).

■ REFERENCES

(1) Zhivaki, D.; Kagan, J. C. Innate Immune Detection of Lipid Oxidation as a Threat Assessment Strategy. *Nat. Rev. Immunol.* **2022**, *22* (5), 322−330.

(2) Adameova, A.; Horvath, C.; Abdul-Ghani, S.; Varga, Z. V.; Suleiman, M. S.; Dhalla, N. S. Interplay of Oxidative Stress and Necrosis-like Cell Death in Cardiac Ischemia/Reperfusion Injury: A Focus on Necroptosis. *Biomedicines* **2022**, *10* (1), No. 127.

(3) Wiernicki, B.; Dubois, H.; Tyurina, Y. Y.; Hassannia, B.; Bayir, H.; Kagan, V. E.; Vandenabeele, P.; Wullaert, A.; Berghe, T. V. Excessive Phospholipid Peroxidation Distinguishes Ferroptosis from Other Cell Death Modes Including Pyroptosis. *Cell Death Dis.* **2020**, *11* (10), No. 922.

(4) Heermeier, K.; Schneider, R.; Heinloth, A.; Wanner, C.; Dimmeler, S.; Galle, J. Oxidative Stress Mediates Apoptosis Induced by Oxidized Low-Density Lipoprotein and Oxidized Lipoprotein(a). *Kidney Int.* **1999**, *56* (4), 1310−1312.

(5) Dong, Y.; Yong, V. W. Oxidized Phospholipids as Novel Mediators of Neurodegeneration. *Trends Neurosci.* **2022**, *45* (6), 419−429.

(6) Seok, J. K.; Hong, E.-H.; Yang, G.; Lee, H. E.; Kim, S.-E.; Liu, K.-H.; Kang, H. C.; Cho, Y.-Y.; Lee, H. S.; Lee, J. Y. Oxidized Phospholipids in Tumor Microenvironment Stimulate Tumor Metastasis via Regulation of Autophagy. *Cells* **2021**, *10* (3), No. 558.

(7) Zhong, S.; Li, L.; Shen, X.; Li, Q.; Xu, W.; Wang, X.; Tao, Y.; Yin, H. An Update on Lipid Oxidation and Inflammation in Cardiovascular Diseases. *Free Radical Biol. Med.* **2019**, *144*, 266−278.

(8) Sottero, B.; Leonarduzzi, G.; Testa, G.; Gargiulo, S.; Poli, G.; Biasi, F. Lipid Oxidation Derived Aldehydes and Oxysterols Between Health and Disease. *Eur. J. Lipid Sci. Technol.* **2019**, *121* (1), No. 1700047.

(9) Fruhwirth, G. O.; Loidl, A.; Hermetter, A. Oxidized Phospholipids: From Molecular Properties to Disease. *Biochim. Biophys. Acta, Mol. Basis Dis.* **2007**, *1772* (7), 718−736.

(10) Greenberg, M. E.; Li, X.-M.; Gugiu, B. G.; Gu, X.; Qin, J.; Salomon, R. G.; Hazen, S. L. The Lipid Whisker Model of the Structure of Oxidized Cell Membranes. *J. Biol. Chem.* **2008**, *283* (4), 2385−2396.

(11) Khandelia, H.; Mouritsen, O. G. Lipid Gymnastics: Evidence of Complete Acyl Chain Reversal in Oxidized Phospholipids from Molecular Simulations. *Biophys. J.* **2009**, *96* (7), 2734−2743.

(12) Runas, K. A.; Malmstadt, N. Low Levels of Lipid Oxidation Radically Increase the Passive Permeability of Lipid Bilayers. *Soft Matter* **2015**, *11* (3), 499−505.

(13) Boonnoy, P.; Jarerattanachat, V.; Karttunen, M.; Wong-ekkabut, J. Bilayer Deformation, Pores, and Micellation Induced by Oxidized Lipids. *J. Phys. Chem. Lett.* **2015**, *6* (24), 4884−4888.

(14) Baxter, A. M.; Wittenberg, N. J. Excitation of Fluorescent Lipid Probes Accelerates Supported Lipid Bilayer Formation via Photosensitized Lipid Oxidation. *Langmuir* **2019**, *35* (35), 11542−11549.

(15) Baxter, A. M.; Jordan, L. R.; Kullappan, M.; Wittenberg, N. J. Tubulation of Supported Lipid Bilayer Membranes Induced by Photosensitized Lipid Oxidation. *Langmuir* **2021**, *37* (19), 5753−5762.

(16) Podrez, E. A.; Poliakov, E.; Shen, Z.; Zhang, R.; Deng, Y.; Sun, M.; Finton, P. J.; Shan, L.; Febbraio, M.; Hajjar, D. P.; Silverstein, R. L.; Hoff, H. F.; Salomon, R. G.; Hazen, S. L. A Novel Family of Atherogenic Oxidized Phospholipids Promotes Macrophage Foam Cell Formation via the Scavenger Receptor CD36 and Is Enriched in Atherosclerotic Lesions. *J. Biol. Chem.* **2002**, *277* (41), 38517−38523.

(17) Gao, D.; Ashraf, M. Z.; Kar, N. S.; Lin, D.; Sayre, L. M.; Podrez, E. A. Structural Basis for the Recognition of Oxidized Phospholipids in Oxidized Low Density Lipoproteins by Class B Scavenger Receptors CD36 and SR-BI. *J. Biol. Chem.* **2010**, *285* (7), 4447−4454.

(18) Ashraf, M. Z.; Kar, N. S.; Chen, X.; Choi, J.; Salomon, R. G.; Febbraio, M.; Podrez, E. A. Specific Oxidized Phospholipids Inhibit

Scavenger Receptor BI-Mediated Selective Uptake of Cholesteryl Esters. *J. Biol. Chem.* **2008**, *283* (16), 10408−10414.
(19) Kar, S.; Tillu, V. A.; Meena, S. C.; Pande, A. H. Closely Related Oxidized Phospholipids Differentially Modulate the Physicochemical Properties of Lipid Particles. *Chem. Phys. Lipids* **2011**, *164* (1), 54−61.
(20) Lv, Z.; Banerjee, S.; Zagorski, K.; Lyubchenko, Y. L. Supported Lipid Bilayers for Atomic Force Microscopy Studies. In *Nanoscale Imaging*; Lyubchenko, Y. L., Ed.; Methods in Molecular Biology; Springer: New York, NY, 2018; Vol. *1814*, pp 129−143.
(21) Parkkila, P.; Elderdfi, M.; Bunker, A.; Viitala, T. Biophysical Characterization of Supported Lipid Bilayers Using Parallel Dual-Wavelength Surface Plasmon Resonance and Quartz Crystal Microbalance Measurements. *Langmuir* **2018**, *34* (27), 8081−8091.
(22) Lind, T. K.; Cárdenas, M.; Wacklin, H. P. Formation of Supported Lipid Bilayers by Vesicle Fusion: Effect of Deposition Temperature. *Langmuir* **2014**, *30* (25), 7259−7263.
(23) Joyce, P.; Jõemetsa, S.; Isaksson, S.; Hossain, S.; Larsson, P.; Bergström, C.; Höök, F. TIRF Microscopy-Based Monitoring of Drug Permeation Across a Lipid Membrane Supported on Mesoporous Silica. *Angew. Chem., Int. Ed.* **2021**, *60* (4), 2069−2073.
(24) Kawakami, L. M.; Yoon, B. K.; Jackman, J. A.; Knoll, W.; Weiss, P. S.; Cho, N.-J. Understanding How Sterols Regulate Membrane Remodeling in Supported Lipid Bilayers. *Langmuir* **2017**, *33* (51), 14756−14765.
(25) Zhang, Y.; Li, Q.; Dong, M.; Han, X. Effect of Cholesterol on the Fluidity of Supported Lipid Bilayers. *Colloids Surf., B* **2020**, *196*, No. 111353.
(26) Beranova, L.; Cwiklik, L.; Jurkiewicz, P.; Hof, M.; Jungwirth, P. Oxidation Changes Physical Properties of Phospholipid Bilayers: Fluorescence Spectroscopy and Molecular Simulations. *Langmuir* **2010**, *26* (9), 6140−6144.
(27) Mendes Ferreira, T.; Sood, R.; Bärenwald, R.; Carlström, G.; Topgaard, D.; Saalwächter, K.; Kinnunen, P. K. J.; Ollila, O. H. S. Acyl Chain Disorder and Azelaoyl Orientation in Lipid Membranes Containing Oxidized Lipids. *Langmuir* **2016**, *32* (25), 6524−6533.
(28) Wong-ekkabut, J.; Xu, Z.; Triampo, W.; Tang, I.-M.; Peter Tieleman, D.; Monticelli, L. Effect of Lipid Peroxidation on the Properties of Lipid Bilayers: A Molecular Dynamics Study. *Biophys. J.* **2007**, *93* (12), 4225−4236.
(29) Du, X.; Fang, J.; Zhu, D.-M. Modified Sauerbrey Equation: A Facile Method to Quantitatively Probe the Conformation of Isolated Molecules at Solid−Liquid Interfaces. *Analyst* **2018**, *143* (13), 3209−3216.
(30) Jönsson, P.; Jonsson, M. P.; Tegenfeldt, J. O.; Höök, F. A Method Improving the Accuracy of Fluorescence Recovery after Photobleaching Analysis. *Biophys. J.* **2008**, *95* (11), 5334−5348.
(31) Wu, E. L.; Cheng, X.; Jo, S.; Rui, H.; Song, K. C.; Dávila-Contreras, E. M.; Qi, Y.; Lee, J.; Monje-Galvan, V.; Venable, R. M.; Klauda, J. B.; Im, W. CHARMM-GUI *Membrane Builder* toward Realistic Biological Membrane Simulations. *J. Comput. Chem.* **2014**, *35* (27), 1997−2004.
(32) Jo, S.; Kim, T.; Iyer, V. G.; Im, W. CHARMM-GUI: A Web-based Graphical User Interface for CHARMM. *J. Comput. Chem.* **2008**, *29* (11), 1859−1865.
(33) Jo, S.; Lim, J. B.; Klauda, J. B.; Im, W. CHARMM-GUI Membrane Builder for Mixed Bilayers and Its Application to Yeast Membranes. *Biophys. J.* **2009**, *97* (1), 50−58.
(34) Klauda, J. B.; Venable, R. M.; Freites, J. A.; O'Connor, J. W.; Tobias, D. J.; Mondragon-Ramirez, C.; Vorobyov, I.; MacKerell, A. D.; Pastor, R. W. Update of the CHARMM All-Atom Additive Force Field for Lipids: Validation on Six Lipid Types. *J. Phys. Chem. B* **2010**, *114* (23), 7830−7843.
(35) Price, D. J.; Brooks, C. L. A Modified TIP3P Water Potential for Simulation with Ewald Summation. *J. Chem. Phys.* **2004**, *121* (20), 10096−10103.
(36) Steinbach, P. J.; Brooks, B. R. New Spherical-cutoff Methods for Long-range Forces in Macromolecular Simulation. *J. Comput. Chem.* **1994**, *15* (7), 667−683.
(37) Essmann, U.; Perera, L.; Berkowitz, M. L.; Darden, T.; Lee, H.; Pedersen, L. G. A Smooth Particle Mesh Ewald Method. *J. Chem. Phys.* **1995**, *103* (19), 8577−8593.
(38) Lee, J.; Cheng, X.; Swails, J. M.; Yeom, M. S.; Eastman, P. K.; Lemkul, J. A.; Wei, S.; Buckner, J.; Jeong, J. C.; Qi, Y.; Jo, S.; Pande, V. S.; Case, D. A.; Brooks, C. L.; MacKerell, A. D.; Klauda, J. B.; Im, W. CHARMM-GUI Input Generator for NAMD, GROMACS, AMBER, OpenMM, and CHARMM/OpenMM Simulations Using the CHARMM36 Additive Force Field. *J. Chem. Theory Comput.* **2016**, *12* (1), 405−413.
(39) Eastman, P.; Swails, J.; Chodera, J. D.; McGibbon, R. T.; Zhao, Y.; Beauchamp, K. A.; Wang, L.-P.; Simmonett, A. C.; Harrigan, M. P.; Stern, C. D.; Wiewiora, R. P.; Brooks, B. R.; Pande, V. S. OpenMM 7: Rapid Development of High Performance Algorithms for Molecular Dynamics. *PLoS Comput. Biol.* **2017**, *13* (7), No. e1005659.
(40) Gao, Y.; Lee, J.; Smith, I. P. S.; Lee, H.; Kim, S.; Qi, Y.; Klauda, J. B.; Widmalm, G.; Khalid, S.; Im, W. CHARMM-GUI Supports Hydrogen Mass Repartitioning and Different Protonation States of Phosphates in Lipopolysaccharides. *J. Chem. Inf. Model.* **2021**, *61* (2), 831−839.
(41) Barth, E.; Kuczera, K.; Leimkuhler, B.; Skeel, R. D. Algorithms for Constrained Molecular Dynamics. *J. Comput. Chem.* **1995**, *16* (10), 1192−1209.
(42) Klauda, J. B.; Brooks, B. R.; Pastor, R. W. Dynamical Motions of Lipids and a Finite Size Effect in Simulations of Bilayers. *J. Chem. Phys.* **2006**, *125* (14), No. 144710.
(43) Ulmefors, H.; Nissa, J.; Pace, H.; Wahlsten, O.; Gunnarsson, A.; Simon, D. T.; Berggren, M.; Höök, F. Formation of Supported Lipid Bilayers Derived from Vesicles of Various Compositional Complexity on Conducting Polymer/Silica Substrates. *Langmuir* **2021**, *37* (18), 5494−5505.
(44) Makky, A.; Tanaka, M. Impact of Lipid Oxidization on Biophysical Properties of Model Cell Membranes. *J. Phys. Chem. B* **2015**, *119* (18), 5857−5863.
(45) Weirich, K. L.; Israelachvili, J. N.; Fygenson, D. K. Bilayer Edges Catalyze Supported Lipid Bilayer Formation. *Biophys. J.* **2010**, *98* (1), 85−92.
(46) Bagheri, B.; Boonnoy, P.; Wong-ekkabut, J.; Karttunen, M. Effect of Oxidation on POPC Lipid Bilayers: Anionic Carboxyl Group Plays a Major Role. *Phys. Chem. Chem. Phys.* **2023**, *25* (27), 18310−18321.
(47) Bhattacharya, S.; Haldar, S. Interactions between Cholesterol and Lipids in Bilayer Membranes. Role of Lipid Headgroup and Hydrocarbon Chain−Backbone Linkage. *Biochim. Biophys. Acta, Biomembr.* **2000**, *1467* (1), 39−53.
(48) Hénin, J.; Chipot, C. Hydrogen-Bonding Patterns of Cholesterol in Lipid Membranes. *Chem. Phys. Lett.* **2006**, *425* (4−6), 329−335.
(49) Štefl, M.; Šachl, R.; Olżyńska, A.; Amaro, M.; Savchenko, D.; Deyneka, A.; Hermetter, A.; Cwiklik, L.; Humpolíčková, J.; Hof, M. Comprehensive Portrait of Cholesterol Containing Oxidized Membrane. *Biochim. Biophys. Acta, Biomembr.* **2014**, *1838* (7), 1769−1776.
(50) Axmann, M.; Schütz, G. J.; Huppa, J. B. Single Molecule Fluorescence Microscopy on Planar Supported Bilayers. *J. Vis. Exp.* **2015**, *104*, No. 53158.
(51) Tero, R.; Yamashita, R.; Hashizume, H.; Suda, Y.; Takikawa, H.; Hori, M.; Ito, M. Nanopore Formation Process in Artificial Cell Membrane Induced by Plasma-Generated Reactive Oxygen Species. *Arch. Biochem. Biophys.* **2016**, *605*, 26−33.
(52) Brown, T. P.; Santa, D. E.; Berger, B. A.; Kong, L.; Wittenberg, N. J.; Im, W. CHARMM GUI Membrane Builder for Oxidized Phospholipid Membrane Modeling and Simulation. *Curr. Opin. Struct. Biol.* **2024**, *86*, No. 102813.
(53) Jurkiewicz, P.; Olżyńska, A.; Cwiklik, L.; Conte, E.; Jungwirth, P.; Megli, F. M.; Hof, M. Biophysics of Lipid Bilayers Containing Oxidatively Modified Phospholipids: Insights from Fluorescence and EPR Experiments and from MD Simulations. *Biochim. Biophys. Acta, Biomembr.* **2012**, *1818* (10), 2388−2402.
(54) Paez-Perez, M.; Vyšniauskas, A.; López-Duarte, I.; Lafarge, E. J.; López-Ríos De Castro, R.; Marques, C. M.; Schroder, A. P.; Muller, P.; Lorenz, C. D.; Brooks, N. J.; Kuimova, M. K. Directly Imaging

Emergence of Phase Separation in Peroxidized Lipid Membranes. *Commun. Chem.* **2023**, *6* (1), 15.
(55) Jeong, H. J.; Picou, C.; Jeong, K.; Chung, J. K. Oxidation Kinetics of Fluorescent Membrane Lipid Peroxidation Indicators. *ACS Chem. Biol.* **2024**, *19*, 1786−1793.
(56) Filippov, A.; Orädd, G.; Lindblom, G. The Effect of Cholesterol on the Lateral Diffusion of Phospholipids in Oriented Bilayers. *Biophys. J.* **2003**, *84* (5), 3079−3086.
(57) Plochberger, B.; Stockner, T.; Chiantia, S.; Brameshuber, M.; Weghuber, J.; Hermetter, A.; Schwille, P.; Schütz, G. J. Cholesterol Slows down the Lateral Mobility of an Oxidized Phospholipid in a Supported Lipid Bilayer. *Langmuir* **2010**, *26* (22), 17322−17329.
(58) Sharma, V. K.; Srinivasan, H.; Gupta, J.; Mitra, S. Lipid Lateral Diffusion: Mechanisms and Modulators. *Soft Matter* **2024**, *20*, 7763−7796.
(59) Schumann-Gillett, A.; O'Mara, M. L. The Effects of Oxidised Phospholipids and Cholesterol on the Biophysical Properties of POPC Bilayers. *Biochim. Biophys. Acta, Biomembr.* **2019**, *1861* (1), 210−219.
(60) Almeida, P. F. F.; Vaz, W. L. C.; Thompson, T. E. Lipid Diffusion, Free Area, and Molecular Dynamics Simulations. *Biophys. J.* **2005**, *88* (6), 4434−4438.
(61) Javanainen, M.; Heftberger, P.; Madsen, J. J.; Miettinen, M. S.; Pabst, G.; Ollila, O. H. S. Quantitative Comparison against Experiments Reveals Imperfections in Force Fields' Descriptions of POPC-Cholesterol Interactions. *J. Chem. Theory Comput.* **2023**, *19* (18), 6342−6352.
(62) Olżyńska, A.; Delcroix, P.; Dolejšová, T.; Krzaczek, K.; Korchowiec, B.; Czogalla, A.; Cwiklik, L. Properties of Lipid Models of Lung Surfactant Containing Cholesterol and Oxidized Lipids: A Mixed Experimental and Computational Study. *Langmuir* **2020**, *36* (4), 1023−1033.

https://doi.org/10.1021/acs.jpcb.4c05451
J. Phys. Chem. B 2024, 128, 11694−11704